symmetry

MDPI

Article

Photo-Induced Relief in Rheology of Liquid Crystals

Dina V. Shmeliova [1], Sergey V. Pasechnik [1,*], Semen S. Kharlamov [1], Alexander V. Dubtsov [1], Alexandre V. Zakharov [1,2], Sarah Loebner [3] and Svetlana Santer [3]

[1] Problem Laboratory of Molecular Acoustics, MIREA-Russian Technological University, 78 Vernadsky Avenue, Moscow 119454, Russia
[2] Saint Petersburg Institute for Machine Sciences, The Russian Academy of Sciences, Saint Petersburg 199178, Russia
[3] Institute of Physics and Astronomy, University of Potsdam, 14476 Potsdam, Germany
* Correspondence: s-p-a-s-m@mail.ru

Abstract: In this paper, we report the first experimental results on capillary shear flows of a nematic liquid crystal 5CB (4-cyano-4′-pentylbiphenyl), arising due to interaction of the anisotropic liquid, correspondent to the continuous rotational symmetry, with photo-profiled polymer surfaces. The regular surface relief was obtained due to opto-mechanical deformation of azobenzene containing potoresponsive polymer film (PAZO) during irradiation with two-beam interference. Such surface treatment makes it possible to obtain a regular submicron profile with well-defined characteristics (direction, period, and height). The polarizing microscopy (PM) and dynamic light scattering (DLS) techniques were used to determine the direction of the surface orientation of LC and anchoring strength, which characterize the interaction of LC with the photo-profiled polymer surface. Two types of shear flows—spreading of LC droplets and capillary flow in a plane capillary, induced by the interaction of LC with one or two photo-profiled surfaces—were investigated for different directions of the flow relative to the direction of the relief. Strong anisotropy in the dynamics of the precursor film and contact line motion, as well as in the dynamical contact angle, was established. The experimental results were analyzed and compared with those previously obtained at the investigation of the spreading of LC droplets over a mechanically stamped submicron profile and capillary flows in plane capillaries with photo-aligned surfaces.

Keywords: liquid crystal; capillary flow; photo-profiled surface; droplet spreading; contact angle; anisotropic shear viscosities; surface relief grating

check for updates

Citation: Shmeliova, D.V.; Pasechnik, S.V.; Kharlamov, S.S.; Dubtsov, A.V.; Zakharov, A.V.; Loebner, S.; Santer, S. Photo-Induced Relief in Rheology of Liquid Crystals. *Symmetry* **2023**, *15*, 722. https://doi.org/10.3390/sym15030722

Academic Editor: P. Ulrich Biedermann

Received: 31 January 2023
Revised: 27 February 2023
Accepted: 7 March 2023
Published: 14 March 2023

Copyright: © 2023 by the authors. Licensee MDPI, Basel, Switzerland. This article is an open access article distributed under the terms and conditions of the Creative Commons Attribution (CC BY) license (https://creativecommons.org/licenses/by/4.0/).

1. Introduction

Liquid crystals (LC) can be considered as a specific class of soft materials showing high sensitivity to the action of external forces. The simplest class of LC—nematic liquid crystals—are characterized by the long-range tensor order parameter Q_{ij}. It includes director $\overrightarrow{n}$, which describes the preferential direction of the long molecular axes, and the scalar order parameter, expressed as a function of the angle declination of the long axis of the individual molecule from $\overrightarrow{n}$, averaged for a large number of molecules. Due to the thermal motion, centrosymmetric ordering is realized, even for the polar molecules, which means that the director can be considered as a continuous axis of the rotational symmetry where the directions $\overrightarrow{n}$ and $-\overrightarrow{n}$ are equivalent to each other. The absence in nematic liquid crystals of the long-ranged translation order results in a high fluidity of LC, similar to that of isotropic liquids. At the same time, such object shows a high degree of anisotropic properties, which is typical for crystals. The combination of the physical properties of crystals and liquids is of special importance for practical applications. In particular, the usage of nematic liquid crystals in the modern display industry is based on a high-sensitivity LC director, preliminarily controlled by specially treated solid surfaces, to the action of electric fields [1]. As the technical parameters of LC devices drastically depend on the interaction of liquid crystal media with solid surfaces, a significant amount

of effort has been paid to obtain surfaces with a perfectly controlled direction of the surface orientation of LC (easy axis) and strength of the interaction (anchoring strength) [2]. The well-known procedure of surface treatment, most used in the display industry, is a rubbing of solid polymer layers formed on glass substrates to obtain a planar type of surface orientation with a well-defined easy axis direction in the plane of the LC layer and a high value of anchoring force. Though such surface treatment has some problems, such as the arising of surface charges, it provides long-term stability of the technical parameters of LC displays, which is of great importance for the operation of LCDs.

Among the different methods of surface treatment developed over the last few decades, photo-alignment technology based on the illumination of photosensitive solid layers by polarized light or UV irradiation provides control of both the surface direction and the anchoring strength, which is of special interest for practical applications [3]. In particular, it makes it possible to realize micro-pattering of a surface and is also applicable for curved surfaces, which can be used, for example, in different photonic devices [4]. Moreover, there is a possibility to change the surface orientation of the LC, not only before, but also after filling the plane capillary with a liquid crystal. In this case, the secondary illumination of photosensitive surfaces with the new direction of the polarization plane results in azimuth rotation of the surface direction to the new state. Such a relatively slow process (gliding of an easy axis) has been intensively studied over the last few decades and has found practical applications in optical rewritable technology [4–6].

Photo-aligned surfaces were also used [7] for the investigation of the shear flows of LC in plane capillaries induced by the pressure gradient (Poiseuille flow). In general, the shear flows of nematics demonstrate non-Newtonian behavior, in particular the dependence of the apparent shear viscosity on the shear rate [8]. Traditionally, strong magnetic fields are used at shear viscosity measurements to suppress the orientational action of flow and surfaces [9]. In this case, liquid crystals can be considered as conventionally Newtonian fluids with a shear viscosity dependent on the field-induced orientation of the director, relative to the flow velocity and velocity gradient [10]. It provides the measurements of three principal shear viscosities of LC (Miesowicz viscosities), which can be expressed via three different combinations of Leslie coefficients entering into the hydrodynamics of the liquid crystals. The given orientation of LC needed for anisotropic shear viscosity measurements can also be achieved by the use of the stabilizing action of the inner surfaces in thin plane capillaries [8].

The interaction of liquid crystals with the solid surface plays the key role in another type of shear flow, induced by wetting phenomena, taking place in the vicinity of the liquid–solid boundary [11]. In the case of one such solid surface, capillary flow manifests itself in the form of a spreading of the droplet placed on the surface. The spreading of liquid droplets over surfaces of various types includes different physical processes [11–14]. Usually, this phenomenon is described in terms of the motion of a contact line and a precursor film arising on the periphery of the droplet, which has a nanometer thickness in the case of isotropic liquids. Therefore, the motion of a precursor film can be considered as the flow of a liquid, which involves the complicated processes of molecular absorption and desorption, taking place at a nanometer scale. At the same time, the motion of the contact line can be described, taking into account the transformation of the initial potential energy of the droplet in the gravity field to the surface energy, arising due to an increase in the square of the liquid–gas interface and the dissipation of energy due to the viscous flow of the liquid. While the spreading of isotropic droplets over surfaces of different types has been investigated in detail, there are only rare experiments and theoretical investigations on the spreading of liquid crystalline droplets [15–20]. In particular, the influence of specific flow instability was observed at the spreading of LC droplets over isotropic surfaces [17]. It has also been shown that polarizing microscopy provides details of the motion dynamics of the contact and precursor lines, as well as changes in the droplet's profile at spreading over the polymer surface with submicron relief, obtained by mechanical stamping [20].

The second type of capillary flow takes place due to the interaction of liquid media with the internal surfaces of a capillary after being filled with a liquid. As in the case of droplet spreading, the dynamical behavior of such flow depends on the values of the contact angle and surface tension coefficient, describing liquid–gas interactions. The results of a detailed investigations of the particular case of a capillary flow—a capillary rise of isotropic Newtonian liquids in vertically oriented capillaries of different cross sections—are presented in [21–23].

Recently, a capillary rise of a nematic liquid crystal in plane capillaries with photo-aligned internal surfaces providing different surface orientations of the LC relative to the capillary flow direction was investigated [24]. Contrary to the mechanical rubbing of the surface, the photo-alignment technique did not induce changes in the submicron relief of the surfaces, which made it possible to study the pure influence of the orientation on the parameters, describing the capillary rise. It was found that the changes in the direction of the surface orientation induced only a minor (approximately 10%) influence on the stationary level of the capillary rise, which was assigned to the weak anisotropy of the contact angle. At the same time, the dynamics of the capillary rise showed higher sensitivity to the direction of the surface orientation, which could be explained by changes in the effective shear viscosity coefficient. The additional application of the electric field suppressed the orientational action of the flow and surfaces, which made it possible to describe the dynamics of the capillary rise in the approximation of conventionally Newton liquid with the maximal value of the shear viscosity.

In this paper, we present the results of experimental investigations of the orientational structure and capillary shear flows of a nematic liquid crystal interacting with photo-profiled polymer surfaces. Such surfaces are generated during the irradiation of azobenzene-containing polymer films with modulated light [25]. The azobenzene molecules attached covalently as side chains to a polymer backbone implement two processes during irradiation: (1) alteration of the surface energy, and thus the wettability of the surface due to photo-isomerization between less polar *trans*- and more polar *cis*-isomers, (2) generation of surface relief gratings (SRG) due to the alignment of the azobenzene groups perpendicular to the electrical field vector and the corresponding generation of local stresses within the polymer film. The latter is realized using two-beam interference lithography, where one generates a periodic local distribution of intensity and/or polarization of incident light. In this way, local ordering of the azobenzene side groups results in re-orientation of the polymer backbone, accompanied by the generation of local stresses, which are then released through macroscopic deformation of the polymer film. The topography of the polymer film mimics the interference pattern and forms a sinusoidally shaped grating of periodicity equal to the optical one [26,27]. By adjusting the irradiation conditions, one can easily control the periodicity and the height of the inscribed grooves [28]. Moreover, depending on the nature of the interference pattern used for inscribing the SRG, one expects different orientations of the polymer chains along the grating period [27]. In the case of illumination with homogeneous light, the topography of the film stays flat, but the surface energy changes drastically, making it possible to manipulate the motion of both isotropic and nematic droplets placed on the surface [29].

This paper is organized as follows. Firstly, we describe the technology of the formation of submicron relief on polymer surfaces and the parameters of that submicron relief on the samples used in the experiments. The results of the measurements of the polymer's optical anisotropy and boundary LC orientation, as well as anchoring strength, which characterize the interaction between the liquid crystal and the surface, are then presented. In the next section, we describe the results of investigations of the dynamics of capillary shear flows, arising both at the spreading of LC droplets over anisotropic photo-profiled surface and the filling of a horizontally oriented plane capillary with a liquid crystal, with the same type of surface treatment. The experimental results are analyzed and compared with those obtained previously after the investigation of the spreading of LC droplets

over a mechanically profiled surface and a capillary flow in plane capillaries with photo-aligned surfaces.

2. Materials and Methods

In our work, we use a polymer of high molecular weight with the azobenzene molecules covalently attached to it as the side chains PAZO (pol{1-[4–(3-carboxy-4-hydroxyphenylazo) benzenesulfonamido]-1,2-ethanediyl,sodiumsalt}). The chemical structure and absorption spectrum are presented in Figure 1a. The samples were pieces of square glass (20 × 20 mm) with a thin layer of PAZO (1.1 μm) deposited by spin-coating technique.

The polymer surface was illuminated according to the technique described in [25] using a ±45° polarization interference pattern. Thus, a round region with a light-induced periodic submicron relief was formed on the surface. The characteristics of the experimental samples with photo-induced relief are presented in Table 1. Figure 1c shows the interference pattern (±45°) used for inscription of the surface relief grating in the polymer films and the according distribution of the polarization of the electric field along the grating vector. Figure 1b shows a diagram representing the principles of submicron relief formation in the interference area.

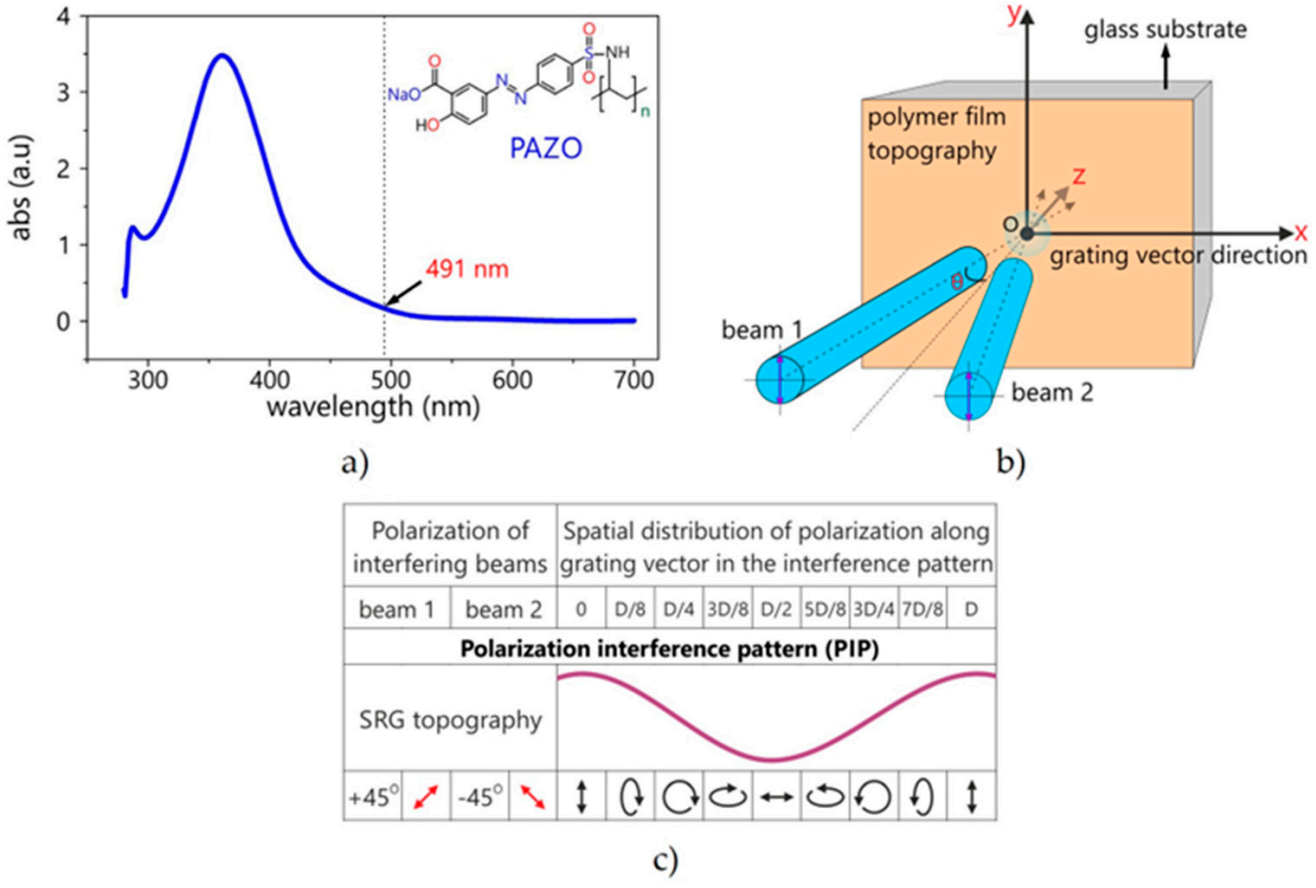

Figure 1. (**a**) UV-Vis absorption spectrum and chemical structure of the photo-responsive polymer (PAZO). The dashed line marks the wavelength (491 nm) used for inscription of the surface relief gratings (SRG). (**b**) Scheme of the sample plane and the grating vector direction (x-axis). The box in the X–Y-plane represents the surface of the polymer film. X–Z is the incidence plane. (**c**) Spatial distributions of polarizations along the grating vector for one optical period. The SRG topography is shown as the magenta curve. The images shown were taken from [25].

Table 1. Characteristics of experimental samples with photo-induced relief.

Sample Number	SRG Height (h, nm)	Relief Period (l, μm)	Irradiated Area with Relief (S, mm^2)
1, 2	200	2	28.3
3, 4	700	4	50.2

The technique described above leads to the formation of local opto-mechanical stress inside the polymer and deformation inside the layer, due to which the relief is formed. In order to determine the effect of this method of creating a relief on the optical properties of the polymer, the exposed samples were examined using the technique of polarization microscopy. The samples were placed between the crossed polarizer and the analyzer. In this case, the sample was initially oriented in the direction of the grooves along the direction of the polarizer transmission plane. The sample was then rotated counterclockwise. After that, the position of the relief relative to the polarizer and analyzer was determined, at which the maximum light transmission was observed.

Thus, it is shown in Figure 2 that, after exposure, the PAZO polymer becomes optically anisotropic, and the optical axis becomes parallel to the direction of the grooves.

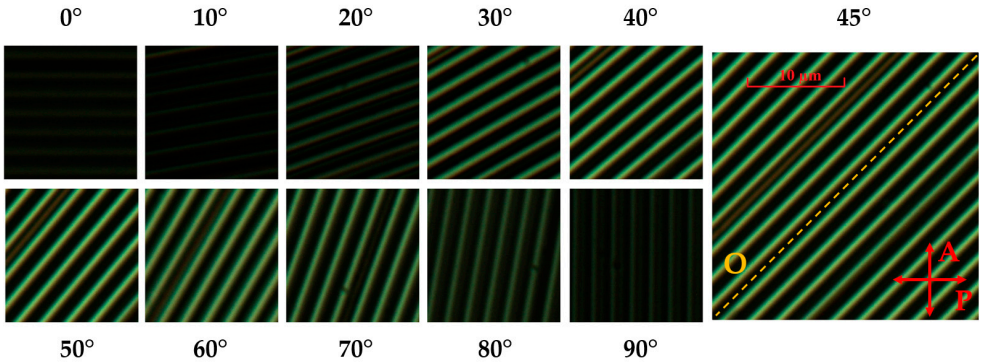

Figure 2. Microscopic images of sample 1 in crossed polarizers. In the initial state, gratings were oriented in the direction of the polarizer's transmission plane. The sample with relief was rotated counterclockwise with 10-degree increments. The 45° image shows the optical axis of the polymer (O).

Previously [20], it has been shown that the surface orientation of the LC was co-directional with the direction of the grooves when interacting with a relief formed by mechanical stamping (l = 0.74 μm, h = 0.15 μm). To check how the LC is oriented on the PAZO surface (both oriented and not), a simple sandwich-like cell was assembled. In this cell (Figure 3a), on one of the surfaces there is a region with a photo-induced relief, and the other surface has a homeotropic surface orientation (the preferential direction of the long axes of the molecules—the director ($\vec{n}$)—is oriented normally with the substrate surface). The gap between the pieces of glass was set by film spacers. The sealing and adjustment of the relative position of the plates was carried out using special clamps. The capillary gap was controlled by the spectrophotometric method.

The homeotropic orientation was created using 0.5% chromolane (chrome stearoyl chloride, Figure 3b) solution in isopropanol, which was spin-coated onto the glass surface and then dried at 100 °C. After the cell was assembled, it was filled with nematic liquid crystal 5CB (4-cyano-4′-pentylbiphenyl, Figure 3c) in the isotropic phase and slowly cooled. Thus, inhomogeneities, associated with the filling of the cell by LC, did not arise. Further studies were carried out at room temperature, T = 23 ± 0.5 °C.

The polarization optical microscopy method described above was also used to determine the surface orientation of the LC on the irradiated PAZO and on the one that was not irradiated. The resulting images are shown in Figure 4.

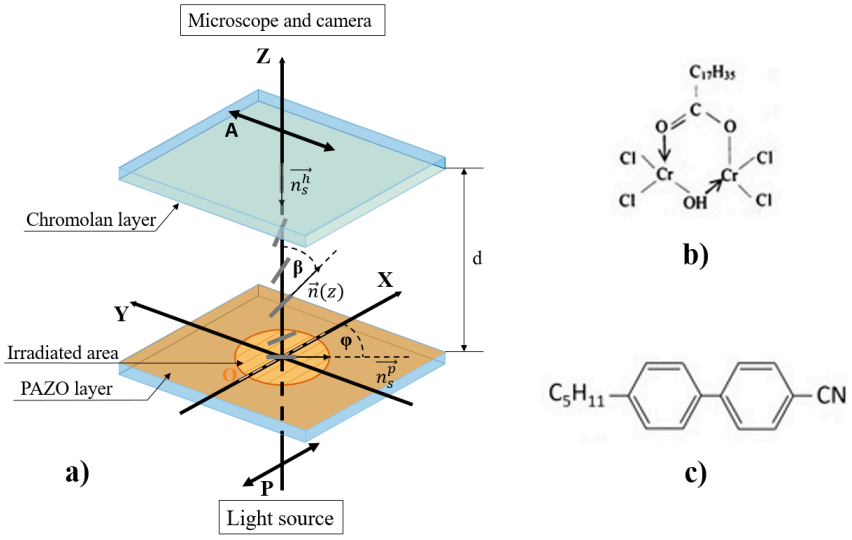

Figure 3. (**a**) Scheme of the cell composed by sample 1 and glass plate with homeotropic surface orientation, gap $d = 15 \pm 1$ μm. Structural formulas of chromolane (**b**) and nematic liquid crystal 5CB (**c**).

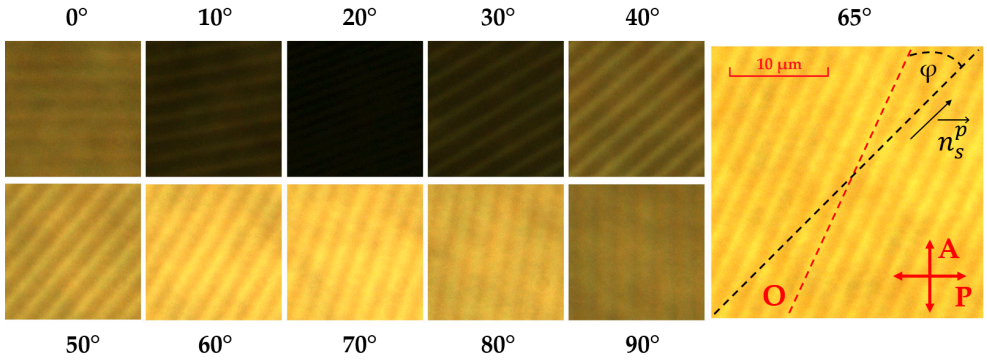

Figure 4. Microscopic images of the cell consisting of sample 1 and the glass plate with homeotropic surface orientation (see Figure 3a, polarizers are crossed). In the initial state, gratings were oriented in the direction of the polarizer's transmission plane. The sample with relief was rotated counter-clockwise with 10° increments. The 65° image shows the optical axis of polymer O and the resulting boundary orientation on SRG ($\overrightarrow{n_s^p}$). The angle φ indicates the deviation of the resulting surface orientation of the LC from the direction of the relief.

The presented images clearly show that the darkest image is observed when the cell is rotated by 20°, and the brightest image is observed when it is rotated by 65°. This indicates that the resulting orientation, $\overrightarrow{n_s^p}$, on the exposed PAZO surface is shifted at an angle $\varphi \approx 20°$ relative to the direction of the grooves. It becomes clear that, in addition to the orienting effect of the grooves, the orientation of the long polymer chains, which are capable of orienting LC, plays an important role.

To measure the anchoring strength of nematic 5CB at the photo-profiled polymer surface, we prepared wedge-like LC cells consisting of two glass plates (reference and tested plates). The reference glass plate was spin-coated with polyimide and rubbed to provide strong anchoring conditions. The tested plate was sample 2. The glass plates with corresponding polymer layers were aligned and sandwiched to provide coincidence of rubbing directions with grooves. A Mylar spacer placed between the glass plates along only one side of the LC cell formed a variable thickness of the LC cell, ranging from 2 to

5.5 μm. The assembled cell was filled with nematic 5CB in an isotropic phase and then slowly cooled to room temperature for DLS measurements.

The anchoring strength of the nematic 5CB on the photo-induced submicron relief surfaces was measured based on a dynamic light scattering technique [30]. For this purpose, we used a photon correlation spectrometer Photocor Complex (LLC Photocor, Russia) to register the autocorrelation function of light intensity fluctuations. In this case, the LC cell was placed and kept in a thermostat of the spectrometer at a temperature of T = 26 °C for 2 h. After incubation, laser light, passing through the LC cell from the side of the reference substrate, was detected by a photomultiplier at a small light scattering angle, λ = 2°. Analysis of the autocorrelation functions was performed using Dyna LS software (LLC Photocor, Moscow, Russia), providing determination of relaxation time, τ, of the autocorrelation function corresponding to the relaxation time of the nematic director fluctuations. We registered autocorrelation function at different values of nematic thickness using two geometries (Figure 5) allowing us to extract both the azimuthal and polar anchoring energies of 5CB at the photo-profiled polymer surfaces.

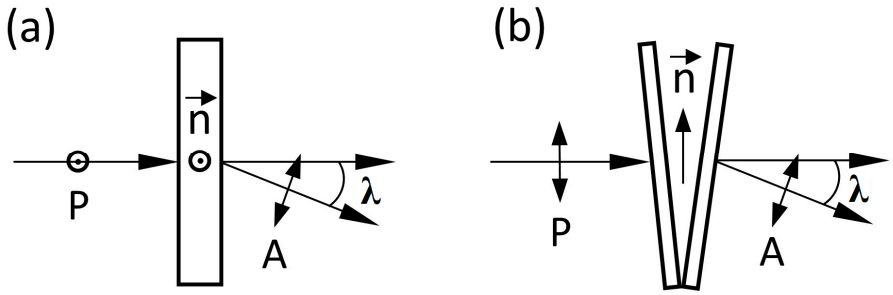

Figure 5. Experimental geometries to measure azimuthal (**a**) and polar (**b**) anchoring strength. The arrows indicate direction of polarizers.

We measured the anchoring energy of nematic 5CB at the photo-profiled polymer surfaces using the dynamic light scattering method, which required no external fields acting on the LC.

Director fluctuations in a bulk NLC can be described by overdamped sinusoidal waves. In unlimited samples, two types of eigenmodes are present: the first one is a combination of splay and bend elastic deformations, and the second a combination of twist and bend deformations. For very thin samples (few microns) and small scattering angles (few degrees), the fundamental mode gives the dominant contribution to the scattered light. The relaxation time of the fundamental mode for infinitely strong anchoring conditions depends only on viscoelastic constants and the sample thickness of the LC [30]:

$$\tau_0 = \frac{\gamma d^2}{K\pi^2}, \tag{1}$$

where γ is the rotational viscosity of LC, d is the LC cell thickness, and K is the nematic elastic module.

To describe strong finite or weak anchoring conditions, the extrapolation length is usually introduced, which is the ratio of the elastic constant to the anchoring strength, $L = K/W$, where W is the anchoring energy. For azimuthal anchoring, $L_a = K_{22}/W_a$, and for polar, $L_p = K_{11}/W_p$, where W_a (W_p) is the azimuthal (polar) anchoring strength and K_{22} (K_{11}) is the twist (splay) LC elastic moduli.

In the case of strong (finite) anchoring, the extrapolation length is much smaller than the sample thickness ($L << d$), and Equation (1) reads as:

$$\tau_0 = \frac{\gamma d^2}{K\pi^2}\left(1 + \frac{4L}{d}\right). \tag{2}$$

For weak anchoring conditions, the extrapolation length, $L >> d$, and the relaxation time of the fundamental mode can be written as:

$$\tau_0 = \frac{\gamma d}{2W}\left(1 + \frac{d}{6L}\right). \quad (3)$$

Therefore, measuring the autocorrelation function using a photon correlation spectrometer, we derived the relaxation time, τ, and estimated the azimuthal/polar anchoring energy of 5CB at the photo-profiled polymer surfaces.

Figure 6 shows the experimental dependence of relaxation time, τ, on nematic thickness, measured with the geometry depicted in Figure 5a.

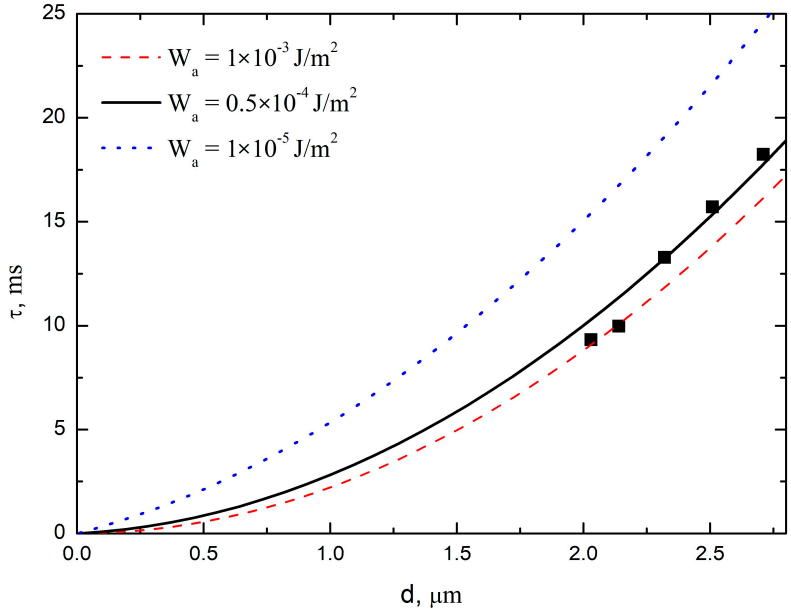

Figure 6. Dependence of the relaxation time, τ, on the LC thickness, d: squares—experimental data; lines—approximation using (2) at different values of azimuthal anchoring energy. Fitting parameters of 5CB: γ = 0.0777 Pa s [31], K_{22} = 3.6 pN [32].

Previously reported results showed that two types of anchoring conditions yielded different dependencies of the relaxation time on sample thickness (linear dependence for weak, and quadratic dependence for strong anchoring) [30]. Figure 6 shows a quadratic dependence of $\tau(d)$, which indicates strong anchoring conditions. Fitting of the presented data using Equation (2) allowed estimation of the azimuthal anchoring strength in the range of 0.5×10^{-4} J/m^2 ... 1×10^{-3} J/m^2. This corresponds to a relatively strong azimuthal anchoring strength of nematic 5CB at submicron relief.

Figure 7 shows the dependence of relaxation time on nematic thickness, measured using the geometry shown in Figure 5b.

Figure 7 shows that polar anchoring strength is in the range of 0.5×10^{-4} J/m^2 ... 1×10^{-3} J/m^2, where best fitting took place at $W_p = 0.5 \times 10^{-4}$ J/m^2.

The presented data indicate that the photo-profiled PAZO film provides a strong azimuthal/polar anchoring strength of nematic 5CB, which is similar to traditional rubbed polymer aligning layers [33].

Investigation of the droplets' spreading over the photo-profiled polymer surfaces was carried out with the help of the polarizing microscopy technique, similar to that used previously for registration of the spreading of LC droplets over the mechanically stamped submicron relief [20]. Figure 8 shows a schematic representation of the position of the drop on the surface of the submicron relief. The sample was illuminated with monochromatic polarized light (semiconductor laser, λ = 650 nm), which provided more correct calculations

of the local thickness of the LC layer in comparison with the use of white light [20]. The crossed polarizers were oriented at an angle 45°, relative to the direction of the submicron relief. The droplets of 5CB with an initial diameter of less than 1 mm were deposited on the submicron relief surface with a micropipette. The microscopic images of the spreading droplets were registered by a digital video camera. Studies were carried out at room temperature, $T = 23 \pm 0.5$ °C.

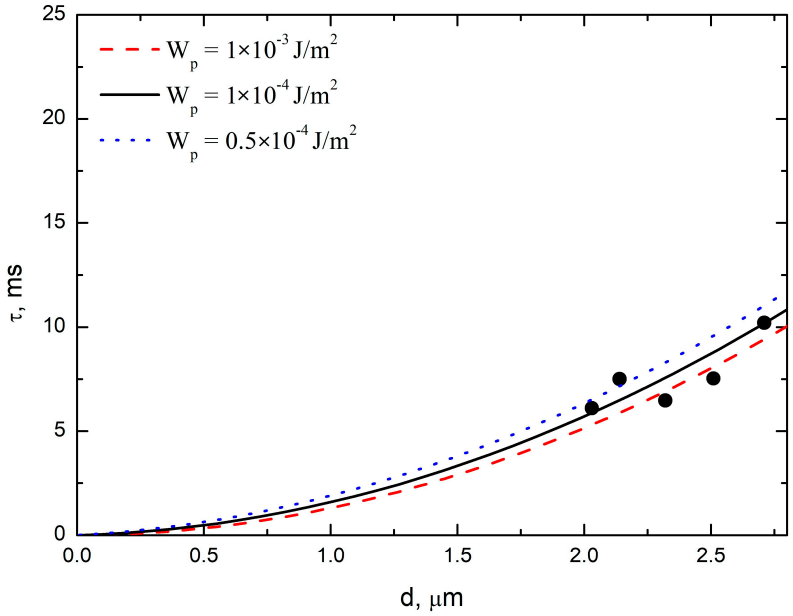

Figure 7. Dependence of the relaxation time, τ, on the cell thickness, d: circles—experimental data; lines—approximation using (2) at different values of polar anchoring energy. Fitting parameters of 5CB: $\gamma = 0.0777$ Pa s [31], $K_{11} = 6.2$ pN [8].

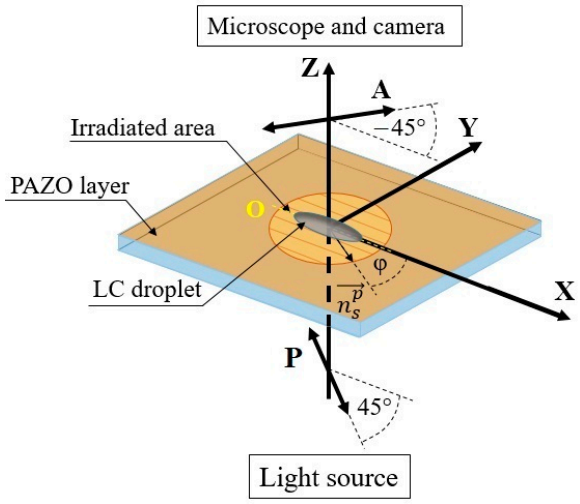

Figure 8. Experimental geometry of LC droplet spreading over the photo-induced relief.

In experiments with a capillary shear flow in a plane capillary, the cells with a construction similar to that shown in Figure 3a were used. The main difference is the use of the photo-profiled inner surfaces on both substrates with the single direction of a relief, as shown in Figure 9.

The design feature of the cell provided measurements of the effective viscosity of LC at different values of the capillary gap at different orientations (parallel and perpendicular)

of the flow direction relative to the direction of the submicron relief. The cell was formed by two flat glass plates with a submicron relief of the same height and period (samples 3 and 4), the gap between them was set by film spacers. The sealing and adjustment of the relative position of the plates was carried out using special clamps. The capillary gap was controlled by the spectrophotometric method at the edges of the capillary and in areas close to the illuminated area.

The scheme of the experiment is similar to that described in [34]; the main difference is that the capillary consists of three regions: a region without a relief at the beginning, a region with a relief, and a region without a relief at the end. Thus, it was possible to observe the movement of the contact line under the action of capillary forces in the cell, where the relief was oriented along flow direction ($\overrightarrow{V^{\parallel}_{flow}}$) and across flow direction ($\overrightarrow{V^{\perp}_{flow}}$).

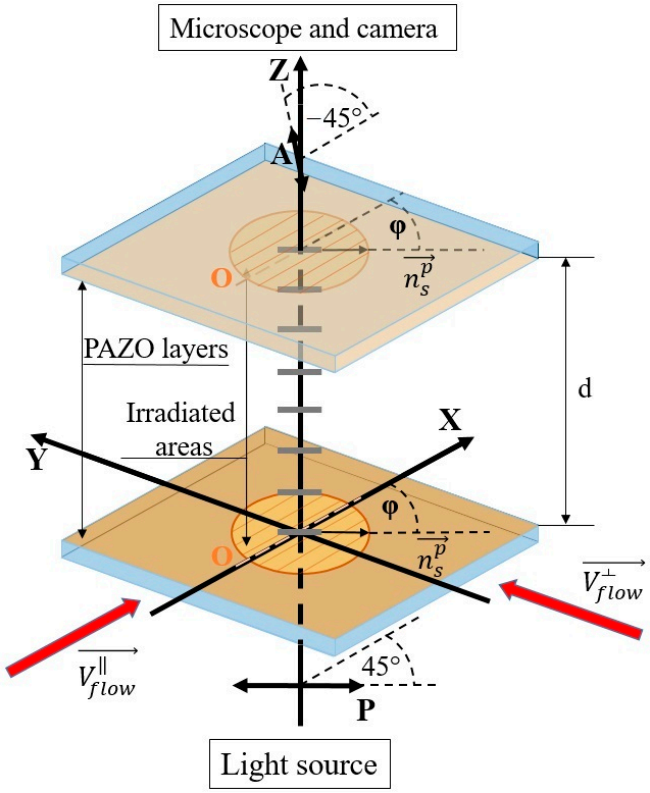

Figure 9. Scheme of the construction of the cells (samples 3 and 4) used in the experiments with a capillary flow of LC, in cases when the flow is directed parallel ($\overrightarrow{V^{\parallel}_{flow}}$) or perpendicular ($\overrightarrow{V^{\perp}_{flow}}$), respectively, to the direction of the grooves.

The capillary flow arose after a portion of the LC was brought into contact with the open edge of the capillary. The instantaneous polarizing images of the cell with the moving meniscus were recorded by a digital camera. The processing of such images was used to study the dynamics of a capillary flow of an LC interacting with the anisotropic photo-profiled surfaces. All experiments were carried out at room temperature, $T = 23 \pm 0.5$ °C.

3. Results and Discussion

The examples of the instant interference images of the droplets for the two experimental cells, with essentially different heights of the submicron relief, are shown in Figure 10. The analysis of the obtained images provided calculation of the local thickness of the LC layer in the vicinity of a contact line.

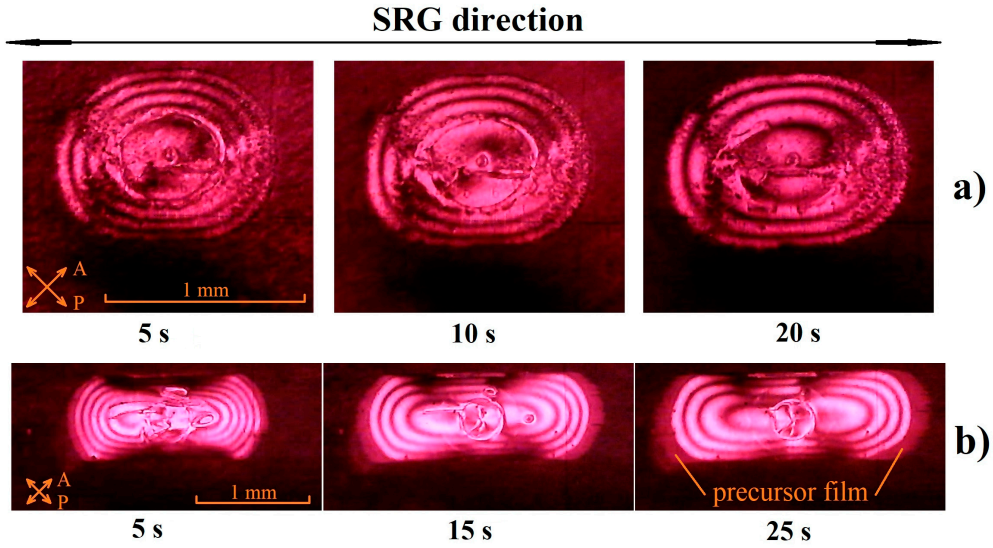

Figure 10. Instant microscopic images of liquid crystal droplets spreading over surfaces with a submicron relief of a different height, h. The photos were taken at different times, after the start of the spreading. The analyzer (A) and polarizer (P) were oriented at +/−45° relative to the direction of the grooves: (**a**) sample 1 with h = 200 nm; (**b**) sample 3 with h = 700 nm.

In order to determine the local thickness (d) in an LC drop, we took into account the dynamic correlation spectroscopy results presented above, which confirmed a rather strong planar anchoring of LC with the photo-induced relief. Similar to the assumption used in [20], the homeotropic orientation is assigned to the air–LC interface (Figure 11). For such a homeoplanar orientation of LC, the simple expression for the polar angle, β, as a function of the z coordinate can be obtained using one constant approximation, $K_{11} \approx K_{33} = K$ (K_{ii} (i = 1 . . . 3) is the Frank elastic constants):

$$\beta(z) = \left(\frac{\pi}{2}\right)\left(1 - \frac{z}{d}\right). \tag{4}$$

The non-zero values of the polar angle result in a phase difference, Φ, between extraordinary (e) and ordinary (o) rays:

$$\Phi = \frac{2\pi}{\lambda}\int_0^d \Delta n(\beta)dz, \tag{5}$$

where $\Delta n(\beta) = n(\beta) - n_0$; the local difference between the extraordinary $n(\beta)$ and ordinary (n_0) refractive indexes, with $n(\beta)$ expressed as:

$$n(\beta) = n_0\left[1 - \frac{n_e^2 - n_0^2}{n_e^2}\cos^2\beta\right]^{-1/2}, \tag{6}$$

where n_e is the maximal value of the extraordinary refractive index.

In the case of a relatively weak optical anisotropy, $\Delta n = n_e - n_0 \ll n_e$, one can obtain the next expression for the phase difference:

$$\Phi = \frac{\pi d}{\lambda}\left[\frac{n_0\left(n_e^2 - n_0^2\right)}{n_e^2}\right], \tag{7}$$

The intensity, I, of polarized light passed through the LC layer can be expressed as:

$$I = I_0 \sin^2 \frac{\Phi}{2}, \tag{8}$$

where I_0 is the intensity of the input light. The presented expressions, (7) and (8), make it possible to restore the instant profiles of a droplet via the analysis of light intensity distribution in the interference pictures, as shown in Figure 10. In particular, the values of the local thickness of LC film, corresponding to interference maxima or minima of the interference pictures, are expressed by Equation (7) or Equation (8):

$$d_k = \left[\frac{\lambda}{2\Delta n}\right](2k+1), \tag{9}$$

$$d_k = \left[\frac{\lambda k}{\Delta n}\right], \tag{10}$$

where k is the number of the extremum. The examples of the instant profiles of the spreading droplet are shown in Figure 11b. The extrapolation of the curves, describing such profiles to the intersection with the surface of the polymer layer, provides determination of the position of a contact line as well as the instant value of a contact angle.

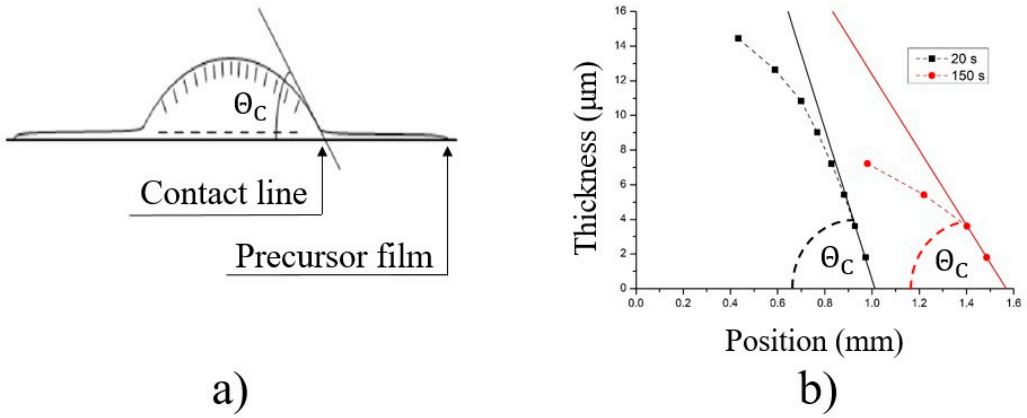

Figure 11. The profile of an LC droplet in the direction of spreading (**a**). The dependence of the local thickness of the 5CB LC drop on position from the center $d(R_S)$ for sample 3 at different moments of time (black squares—20 s after the start of spreading; red circles—150 s, (**b**)).

The dependences of the contact angle on time at two principal orientations of the flow velocity relatively to the direction of a relief (parallel and perpendicular to the groves) for the samples with the different values of the height of a relief are shown in Figure 12. One can observe the relatively fast decreasing of the contact angle at the initial stage of spreading, slowly approaching to the stationary value at the final stage. The range of variation of this parameter with time from 3.0° to 1.5° in the direction of spreading parallel to the grooves is close to the range (from 5.0° to 2.2°) obtained at similar experiments with the spreading of an LC droplet over a mechanically stamped relief with the close value (approximately 150 nm) of the relief height. Comparison between the results obtained for different samples reveals the essential increase in the anisotropy of the dynamical contact angle with the increase in the height of a relief (see Figure 12). It is worth noting that the character of motion of the precursor line also strongly depends on the height of the relief. In particular, in the comparison with the relatively large distant between the positions of a contact and precursor lines, observed at spreading along the relief with large height, this distance is essentially lower at the spreading of the LC droplet over a relief with the smaller height, and in the photographs it almost does not differ from the movement of the contact line.

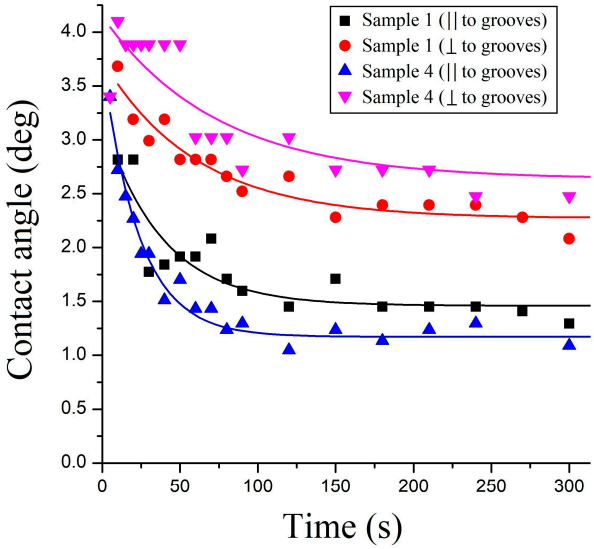

Equation	$\Theta_C(t) = \Theta_{C0} + \Theta_{C1} \times \exp(-t/\tau)$			
Reduced Chi-Sqr	0.04633	0.0177	0.0124	0.07991
Adj. R-Square	0.77762	0.89867	0.96964	0.74418
		Value	Standard Error	
	Θ_{C0}	1.46001	0.09034	
	Θ_{C1}	1.74204	0.3084	
	τ	37.65862	11.04673	
	Θ_{C0}	2.26954	0.07392	
	Θ_{C1}	1.47116	0.14115	
	τ	60.75221	12.98661	
	Θ_{C0}	1.17154	0.03469	
	Θ_{C1}	2.57284	0.13925	
	τ	23.46305	2.14514	
	Θ_{C0}	2.63474	0.13293	
	Θ_{C1}	1.51116	0.19989	
	τ	73.81773	25.43107	

Figure 12. Time dependences of contact angle, $\Theta_C(t)$, value during the spreading of the LC droplet on irradiated PAZO film for sample 1 (parallel to the grooves direction—black squares, perpendicular to the grooves direction—red circles) and sample 3 (parallel to the grooves direction—blue triangles, perpendicular to the grooves direction—purple triangles). Solid lines with corresponding colors show simple exponential approximation with function $\Theta_C(t) = \Theta_0 + \Theta_1 \times \exp(-t/\tau)$. Approximation parameters are shown in the figure.

In the case of an LC drop spreading over the surface of a sample with a lower relief height (sample 1), the contact line moved in a direction perpendicular to the direction of the grooves only at the very beginning of spreading (the first few seconds), while for samples with a sufficiently large relief height (sample 3), spreading in the direction normal to the relief direction was not observed at all. Figure 13 shows normalized to the initial droplet size time dependences of the displacement of the contact and precursor lines along the direction of the relief for samples 1 and 3.

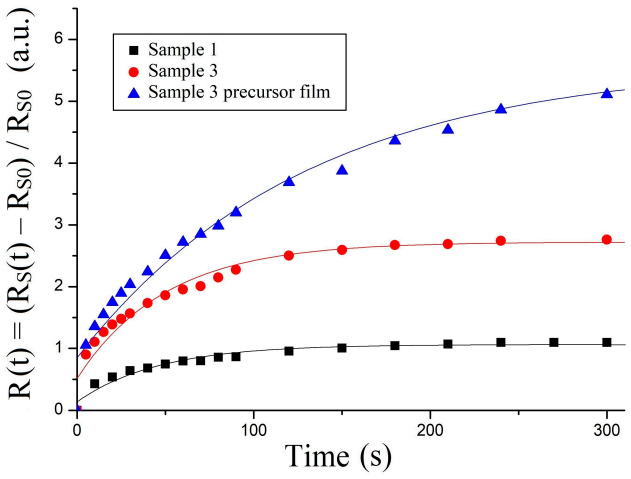

Equation	$R(t) = R_0 + R_1 \times \exp(-t/\tau)$		
Reduced Chi-Sqr	0.00413	0.02484	0.05775
Adj. R-Square	0.95139	0.95642	0.97756
		Value	Standard Error
	R_0	1.06437	0.02871
	R_1	-0.92683	0.05346
	τ	46.14354	5.77439
	R_0	2.72348	0.06083
	R_1	-2.20726	0.10577
	τ	50.27662	5.75915
	R_0	5.61571	0.17562
	R_1	-4.76572	0.17325
	τ	128.7806	13.60813

Figure 13. Normalized to the initial droplet size (R_{S0}), time dependences (R(t)) of the displacement of the contact (sample 1—black squares, sample 3—red circles) and precursor (sample 3—blue triangles) lines along the direction of the relief. Solid lines with corresponding colors show simple exponential approximation with function $R(t) = R_0 + R_1 \times \exp(-t/\tau)$. Approximation parameters are shown in the figure.

A similar experiment on the spreading of an LC drop over the surface of an unexposed PAZO showed that the drop spreads as though it were an isotropic surface and does not have a preferred spreading direction. At the same time, interference fringes are observed in crossed polarizers along the direction of the analyzer and polarizer transmission planes, which makes it possible to similarly estimate the contact angle at the LC–PAZO interface. In our case, it turned out to be equal to 20° at the beginning of spreading and 15° at the end of spreading.

Using Equations (7) and (8), as well as digital image processing, the local thickness of the precursor film was determined using the ratio of the light intensities in the region of the precursor film and the region of maximum of interference. The value of the local thickness in the precursor film was equal to 1 μm near the main mass of the drop and 0.4 μm at the boundary of the precursor.

The results of the investigation of the dynamics of the capillary flow in plane capillaries were also obtained due to the processing of instant photos. The examples of such photos, taken at the usage of white polarized light, are presented in Figure 14. The motion of the meniscus is well visualized, which makes it possible to determine the displacement of a contact line with time. The corresponding results for two orthogonal orientations of the capillary flow relative to the direction of a relief are shown in Figure 15. The wide interference lines on the image can be assigned to the weak space variations of the thickness of the LC layer contacted with the relief surface. At the same time, there is no evidence of flow-induced changes of the initial orientation. This means that the photo-induced relief can be used for stabilization of LC orientation, which is important for shear viscosity measurements.

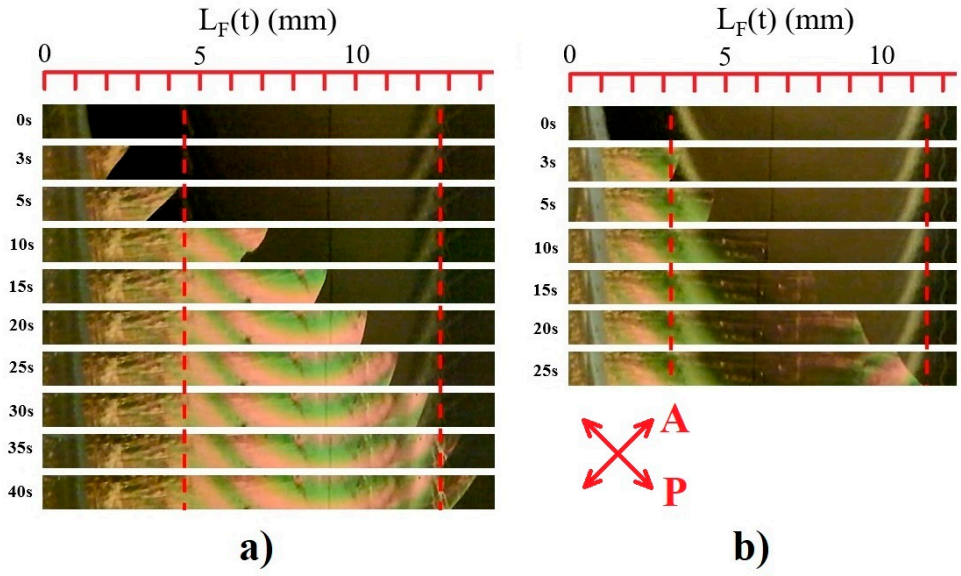

Figure 14. Snapshots showing the movement of a contact line in capillaries consisting of samples 3 and 4. Polarizer and analyzer are crossed and oriented at 45° relative to the flow direction: (**a**) grooves are perpendicular to the flow velocity gradient ($\overrightarrow{V^{\perp}_{flow}}$); (**b**) grooves are parallel to the flow velocity gradient ($\overrightarrow{V^{\parallel}_{flow}}$). The red dashed lines show the position of the beginning and end of the relief.

Therefore, when processing the data on the capillary flow in a cell with two photo-induced substrates (Figure 14), we assumed, similarly to [34], that LC is a conventional Newtonian liquid with a constant value of the shear viscosity coefficient (η), which depends on the director's orientation respective to the flow velocity direction and velocity gradient.

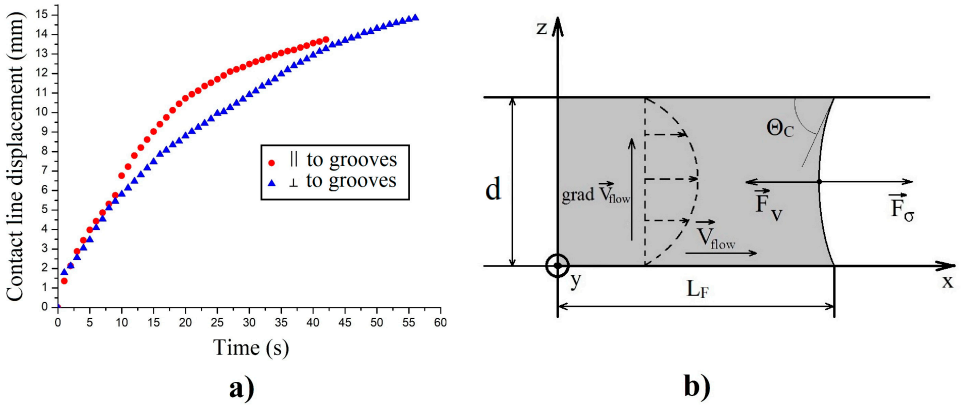

Figure 15. (**a**) Time dependences of the displacement of the contact line $L_F(t)$ for a sample consisting of cells 3 and 4, gap $d = 15 \pm 1$ μm. Red circles—the direction of the flow velocity ($\overrightarrow{V^{\parallel}_{flow}}$) is parallel to the direction of the grooves, blue triangles—the direction of the flow velocity ($\overrightarrow{V^{\perp}_{flow}}$) is perpendicular to the direction of the grooves. (**b**) Scheme illustrating the capillary flow of the LC under the action of capillary ($\overrightarrow{Fc}$) and viscous ($\overrightarrow{Fv}$) forces.

We also considered the contact angle as a constant value, which is time-independent. It holds at small values of the capillary number [21]:

$$Ca = \frac{\eta v}{\sigma} \ll 1, \tag{11}$$

where $v = dl/dt$ is the velocity of the contact line and σ is the surface tension coefficient.

Using the values $\sigma = 0.03$ N/m and $\eta = 0.1$ Pa s (maximal at corresponding temperature) for a 5CB liquid crystal [10] and obtained value of $v < 10$ mm/s at the initial stage of capillary flow, we obtain capillary number Ca = 0.003, which allows us to consider the contact angle as a constant.

The above-mentioned approximations make it possible to describe the displacement of the contact line in a horizontally oriented capillary. The pressure balance expression obtained by taking into account only the capillary (F_σ) and the viscous (F_v) forces, acting on the sample of LC (Figure 15b), can be written as:

$$P_\sigma = P_v, \tag{12}$$

where

$$P_\sigma = \frac{2\sigma cos\Theta_C}{d} \tag{13}$$

is the capillary pressure, and

$$P_v = \left(\frac{12\eta L_F}{d^2}\right)\left(\frac{dL_F}{dt}\right) \tag{14}$$

is the pressure drop caused by viscosity losses during the laminar flow of a liquid through the plane capillary; η is the shear viscosity of a liquid. This expression is derived with the help of the formula $Q = dV/dt$, describing the volumetric flow rate of liquid during a steady Poiseuille flow through a capillary with a gap d, width A, and length L:

$$Q = \left[\frac{d^3 A}{12\eta}\right]\left(\frac{P_v}{L_F}\right). \tag{15}$$

By inserting (13) and (14) into expression (12), it is simple to obtain the next differential equation for $L_F(t)$:

$$L_F\left(\frac{dL_F}{dt}\right) = \frac{d\sigma cos\Theta_C}{6\eta}. \quad (16)$$

The solution of Equation (15) leads to the linear dependence of L_F^2 on time, written as:

$$L_F^2(t) = \left[\frac{d\sigma cos\Theta_C}{3\eta}\right]t. \quad (17)$$

As can be seen in Figure 16, three sections can be considered (the area before the relief, the area with the relief, the area after the relief). The corresponding values of the effective viscosity are 0.051 ± 0.004 Pa·s for the untreated areas before and after the relief (Figure 16a,b). For the area with relief in the case when flow direction was parallel to the grooves orientation, the value of shear viscosity was equal to 0.024 ± 0.002 Pa·s (Figure 16b). This is close to the minimum Miesowicz viscosity for the given temperature of the experiment (η_2 = 0.023 Pa·s [10]) for the case when the director is oriented along the flow. For the case when the flow is directed perpendicular to the direction of the relief (Figure 15a), an effective shear viscosity in the area with relief was 0.037 ± 0.002 Pa·s, which is close to the Miesowicz viscosity η_3 = 0.033 Pa·s, corresponding to the orientation of the director perpendicular to the flow plane. Thus, at small thicknesses of the LC layer, the surface stabilizes the orientational structure of the liquid crystal, which makes it possible to use the capillaries with photo-profiled surfaces at the experimental determination of anisotropic shear viscosities of liquid crystals.

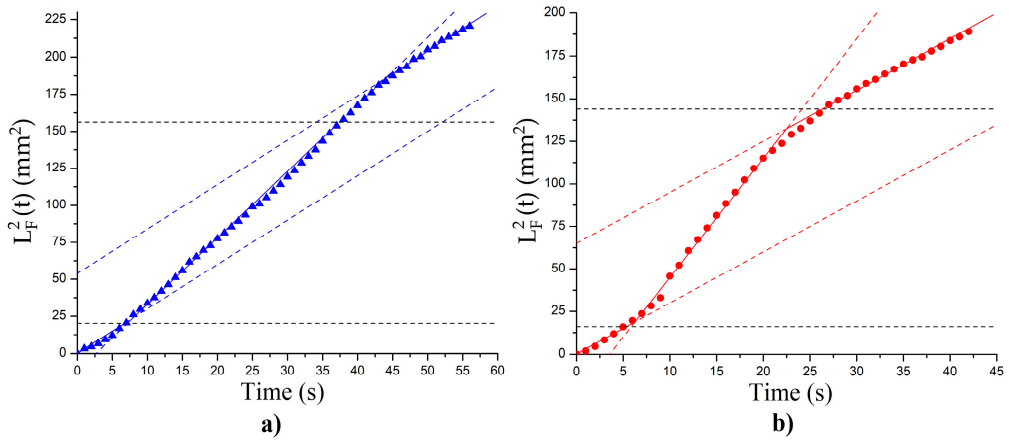

Figure 16. Time dependences of the parameter $L_F^2(t)$: (**a**) the direction of the flow velocity ($\overrightarrow{V_{flow}^{\perp}}$) is perpendicular to the direction of the grooves; (**b**) the direction of the flow velocity ($\overrightarrow{V_{flow}^{\parallel}}$) is parallel to the direction of the grooves. Colored lines show a linear approximation according to Equation (17). Black dashed lines show the beginning and end of the relief area.

Finally, we have to point out that, in spite of the general nature of the two types of capillary flow described above, they also demonstrate differences in dynamics. In particular, simple time dependence (17) for a contact line motion in plane capillaries does not hold for the anisotropic spreading of LC droplets. This may be connected with the different roles of free surfaces in the phenomenon, as mentioned above. In particular, the changes in the area of the free surface inside a capillary are connected only with the dynamic changes of the contact angle and can be neglected in our case. At the same time, such changes can essentially exceed the initial area of the free surface of the spherical droplet placed on the surface. This means that variation of the free surface area with time plays a key role in droplet spreading. Additionally, the influence of changes in the gravity energy of a droplet, taking place at spreading, also modifies the dynamics of spreading. The detailed analysis

of anisotropic motion of the precursor line, registered in our experiments, demands the use of a mesoscopic or microscopic theoretical description. In particular, the performed molecular dynamical simulation of the kinetics of spreading of isotropic nano-droplets over submicron relief surfaces of different topologies [35] made it possible to determine the time dependence of the precursor film displacement, similar to that shown in Figure 15. We hope that the presented experimental results will also stimulate microscopic theoretical investigations for the spreading of LC droplets.

4. Conclusions

The first experimental investigation of the shear flows of a liquid crystal (LC) induced by capillary forces, arising due to the interaction of LC with photo-profiled polymer surfaces, were fulfilled. Such surfaces are characterized by the well-defined parameter of a submicron relief. Two types of capillary shear flows were under investigation. The first type is the spreading of an LC droplet over photo-profiled polymer surfaces, when anisotropic liquid interacts with one solid surface, while the second type—capillary flow—arises due to interaction of the LC with the two photo-profiled inner surfaces, which results in the filling of a plane capillary with an anisotropic liquid. In the latter case, the changes in the area of the free surface can have some influence on the dynamics of the capillary flow due to the corresponding time dependence of the contact angle. At the same time, the mentioned above changes of the free surface area essentially determine the dynamics of the spreading, as well as the final stationary state of the droplet's shape. The influence of the direction and the height of the regular surface relief on the dynamics of the capillary flows mentioned above was experimentally studied, analyzed, and compared with the previously obtained results of the investigations of a droplet's spreading over mechanically stumped submicron relief and capillary rise in plane capillaries with photo-aligned surfaces. In summary, we note the following results:

1. The direction of the surface orientation of a liquid crystal, which contacts with the photo-profiled polymer surfaces, is declined (at an angle of approximately 20°) from the direction of the relief, which is different from the case of a mechanically stamped submicron relief, where these directions coincide. This indicates the role of intermolecular interactions between the LC and the polymer substrate, where non homogeneous orientation of the polymer chain can arise due to specific types of polarization.
2. The experimentally measured values of the polar and azimuth anchoring strength correspond to the rather strong surface anchoring between the LC and photo-profiled surfaces, which may be important for the practical application of such surfaces in photonics.
3. The anisotropy in the spreading of LC droplets was established, which is similar to the results obtained for a mechanically stamped relief. The obtained values of the contacts angle (2 ... 4°) in the direction of a relief correspond to the good wetting of the surface. They are essentially lower than the values (15 ... 20°) measured for non-treated surfaces. This, along with optically induced anisotropy of a contact angle, can be used in microfluidic applications, because micro-pattering of the surface is made possible by using the surface treatment described above.
4. To describe the dynamics of the liquid crystal capillary flow, a theoretical model of the capillary flow of a conventionally Newtonian liquid was applied. The results, obtained after investigation of a capillary flow of an LC in plane capillaries, show the different dynamics of the capillary flow in the direction of the relief and in the direction normal to the relief, which can be assigned to the anisotropy of the shear viscosity. In the case of small thicknesses (approximately 15 μm) of the LC layer, we did not observe essential flow-induced changes of LC orientation. Therefore, the approximation of a conventionally Newtonian liquid is valid, which makes it possible to use capillaries with photo-profiled surfaces for experimental determination of the anisotropic shear viscosities of liquid crystals.

Author Contributions: D.V.S., S.S.K. and A.V.D. performed the experiments and analyzed the obtained data of dynamic light scattering method, optical microscopy images, and the behavior of LC on the surface of the polymer and in the capillary channel. S.L. prepared experimental samples and characterized them. S.V.P., A.V.Z. and S.S. supervised the study. All authors wrote and reviewed the manuscript. All authors have read and agreed to the published version of the manuscript.

Funding: This work was supported by the Ministry of Education and Science of the Russian Federation (Grant № FSFZ-2023-0004). The reported study was also funded by the Russian Foundation for Basic Research (RFBR and DFG project № 20-52-12040).

Data Availability Statement: Not applicable.

Conflicts of Interest: The authors declare no conflict of interest.

References

1. Yakovlev, D.A.; Chigrinov, V.G.; Kwok, H.-S. *Modeling and Optimization of LCD Optical Performance*; John Wiley & Sons Ltd.: Chichester, UK, 2015; p. 584.
2. Takatoch, K.; Hazegawa, M.; Koden, M.; Itoh, N.; Hazekawa, R.; Sakamoto, M. *Alignment Technologies and Applications of Liquid Crystal Devices*; Taylor and Francis: London, UK, New York, NY, USA; 2005; p. 263.
3. Chigrinov, V.G.; Kozenkov, V.M.; Kwok, H.-S. *Photoalignment of Liquid Crystalline Materials: Physics and Applications*; Wiley: New York, NY, USA, 2008; p. 231.
4. Chigrinov, V.G. *Liquid Crystal Photonics (Engineering Tools, Techniques and Tables)*; Nova Science Pub Inc.: Hauppauge, NY, USA, 2014; p. 204.
5. Vorflusev, V.P.; Kitzerow, H.S.; Chigrinov, V.G. Azimuthal Surface Gliding of a Nematic Liquid Crystal. *Appl. Phys. Lett.* **1997**, *70*, 3359–3361. [CrossRef]
6. Dubtsov, A.V.; Pasechnik, S.V.; Kiselev, A.D.; Shmeliova, D.V.; Chigrinov, V.G. Effects of polarization azimuth in dynamics of electrically assisted light-induced gliding of nematic liquid-crystal easy axis. *Appl. Phys. Lett.* **2012**, *100*, 141608. [CrossRef]
7. Pasechnik, S.V.; Shmeliova, D.V.; Kharlamova (Semina), O.A.; Chigrinov, V.G.; Jiatong, S.; Dubtsov, A.V. Photoalignment in rheology of liquid crystals. *Mol. Cryst. Liq. Cryst.* **2012**, *560*, 131–142. [CrossRef]
8. Pasechnik, S.V.; Chigrinov, V.G.; Shmeliova, D.V. *Liquid Crystals: Viscous and Elastic Properties*; WILEY-VCH Verlag GmbH & Co. KGaA: Weinheim, Germany, 2009; p. 424.
9. Kneppe, H.; Schneider, F. Viscosity. In *Handbook of Liquid Crystals*; Demus, D., Goodby, J., Gray, G.W., Spiess, H.-W., Vill, V., Eds.; Wiley-VCH Verlag: Weinheim, Germany, 1998; pp. 142–169.
10. Stewart, I.W. *The Static and Dynamic Continuum Theory of Liquid Crystals: A Mathematical Introduction*; Tailor and Francis: Abingdon, UK, 2004; p. 351.
11. de Gennes, P.G. Wetting: Statics and dynamics. *Rev. Mod. Phys.* **1985**, *57*, 827–863. [CrossRef]
12. Bénichou, O.; Cachile, M.; Cazabat, A.M.; Poulard, C.; Valignat, M.P.; Vandenbrouck, F.; Van Effenterre, D. Thin films in wetting and spreading. *Adv. Colloid Interface Sci.* **2003**, *100*, 381–398. [CrossRef]
13. Adão, M.H.; de Ruijter, M.; Voué, M.; De Coninck, J. Droplet spreading on heterogeneous substrates using molecular dynamics. *Phys. Rev. E* **1999**, *59*, 746–750. [CrossRef]
14. Cheng, E.; Ebner, C. Dynamics of liquid-droplet spreading: A Monte Carlo study. *Phys. Rev. B* **1993**, *47*, 13808–13811. [CrossRef]
15. Cummings, L.J.; Lin, T.-S.; Kondic, L. Modeling and simulations of the spreading and destabilization of nematic droplets. *Phys. Fluids.* **2011**, *23*, 043102–043112. [CrossRef]
16. Bardon, S.; Ober, R.; Valignat, M.P.; Vandenbrouck, F.; Cazabat, A.M.; Daillant, J. Organization of cyanobiphenyl liquid crystal molecules in prewetting films spreading on silicon wafers. *Phys. Rev. E* **1999**, *59*, 6808–6818. [CrossRef]
17. Poulard, C.; Cazabat, A.M. Spontaneous spreading of nematic liquid crystals. *Langmuir* **2005**, *21*, 6270–6276. [CrossRef]
18. Rey, A.D. Nematic contact lines and the Neumann and Young equations for liquid crystals. *J. Chem. Phys.* **1999**, *111*, 7675–7684. [CrossRef]
19. Viswanath, P.; Suresh, K.A. Spreading and retraction dynamics of smectic liquid crystal domains at interfaces. *Liq. Cryst.* **2014**, *41*, 320–327. [CrossRef]
20. Shmeliova, D.V.; Tsvetkov, V.A.; Pasechnik, S.V.; Kozenkov, V.M.; Dorozhkina, G.N.; Angelutz, A.A.; Lezhnev, A.V. Anisotropic spreading of liquid crystals and isotropic fluids on anisometric surface of DVD discs. *Mol. Cryst. Liq. Cryst.* **2008**, *495*, 212–564. [CrossRef]
21. Heshmati, M.; Piri, M. Experimental Investigation of Dynamic Contact Angle and Capillary Rise in Tubes with Circular and Noncircular Cross Sections. *Langmuir* **2014**, *30*, 14151–14162. [CrossRef]
22. Ponomarenko, A.; Quere, D.; Clanet, C. A Universal Law for Capillary Rise in Corners. *J. Fluid Mech.* **2011**, *666*, 146–154. [CrossRef]
23. Dreyer, M.; Delgado, A.; Rath, H.-J. Capillary Rise of Liquid between Parallel Plates under Microgravity. *J. Colloid Interface Sci.* **1994**, *163*, 158–168. [CrossRef]

24. Shmeliova, D.V.; Pasechnik, S.V.; Kharlamov, S.S.; Zakharov, A.V.; Pozhidaev, E.P.; Barbashov, V.A.; Tkachenko, T.P. Capillary Flows of Nematic Liquid Crystal. *Crystals* **2020**, *10*, 1029. [CrossRef]
25. Yadavalli, N.S.; Saphiannikova, M.; Santer, S. Photosensitive response of azobenzene containing films towards pure intensity or polarization interference patterns. *Appl. Phys. Lett.* **2014**, *105*, 051601. [CrossRef]
26. Toshchevikov, V.; Ilnytskyi, J.; Saphiannikova, M. Photoisomerization kinetics and mechanical stress in azobenzene-containing materials. *J. Phys. Chem. Lett.* **2017**, *8*, 1094–1098. [CrossRef]
27. Tverdokhleb, N.; Loebner, S.; Yadav, B.; Santer, S.; Saphiannikova, M. Viscoplastic Modeling of Surface Relief Grating Growth on Isotropic and Preoriented Azopolymer Films. *Polymers* **2023**, *15*, 463. [CrossRef]
28. Yadavalli, N.S.; Saphiannikova, M.; Lomadze, N.; Goldenberg, L.M.; Santer, S. Structuring of photosensitive material below diffraction limit using far field irradiation. *Appl. Phys. A* **2013**, *113*, 263–272. [CrossRef]
29. Umlandt, M.; Kopyshev, A.; Pasechnik, S.V.; Zakharov, A.V.; Lomadze, N.; Santer, S. Light-Triggered Manipulations of Droplets All in One: Reversible Wetting, Transport, Splitting, and Merging. *ACS Appl. Mater. Interfaces* **2022**, *14*, 41412–41420. [CrossRef] [PubMed]
30. Vilfan, M.; Mertelj, A.; Copic, M. Dynamic light scattering measurements of azimuthal and zenithal anchoring of nematic liquid crystals. *Phys. Rev. E* **2002**, *65*, 041712. [CrossRef]
31. Kneppe, H.; Schneider, F.; Sharma, N.K. Rotational viscosity $\gamma 1$ of nematic liquid crystals. *J. Chem. Phys.* **1982**, *77*, 3203–3208. [CrossRef]
32. Toyooka, T.; Chen, G.-P.; Takezoe, H.; Fukuda, A. Fukuda Determination of Twist Elastic Constant K22 in 5CB by Four Independent Light-Scattering Techniques. *Jpn. J. Appl. Phys.* **1987**, *26*, 1959–1966. [CrossRef]
33. Rasing, T.; Muševič, I. *Surfaces and Interfaces of Liquid Crystals*; Springer: Berlin/Heidelberg, Germany, 2004; p. 296.
34. Shmeliova, D.V.; Pozhidaev, E.P.; Kharlamov, S.S.; Pasechnik, S.V.; Barbashov, V.A.; Chigrinov, V.G. Capillary flow and shear viscosity of ferroelectric liquid crystal. *Liq. Cryst. Appl.* **2018**, *18*, 88–94. [CrossRef]
35. Samsonov, V.M.; Dronnikov, V.V.; Volnukhina, A.A.; Muravyev, S.D. Molecular dynamical simulation of structure formation after nanodroplet spreading over heterogeneous surfaces. *Surf. Sci.* **2003**, *532*, 560–566. [CrossRef]

Disclaimer/Publisher's Note: The statements, opinions and data contained in all publications are solely those of the individual author(s) and contributor(s) and not of MDPI and/or the editor(s). MDPI and/or the editor(s) disclaim responsibility for any injury to people or property resulting from any ideas, methods, instructions or products referred to in the content.